

# Universal Distribution of Non-Fickian Particle Kinetics in Three-Dimensional Porous Media

Dian Fan,<sup>1,\*</sup> Ronny Pini,<sup>2</sup> and Alberto Striolo<sup>1,†</sup>

<sup>1</sup>*Department of Chemical Engineering, University College London, London WC1E 7JE, UK.*

<sup>2</sup>*Department of Chemical Engineering, Imperial College London, South Kensington Campus, London SW7 2AZ, UK.*

(Dated: December 22, 2024)

We study particle transport in three-dimensional random packings of monodispersed spheres at different particle Péclet numbers using Lagrangian simulations. We find a universal non-exponential function that describes the observed particle velocity probability distributions when non-Fickian behavior occurs. The function also reproduces results from particle tracking experiments and yields the Maxwell-Boltzmann distribution in the Fickian limit. We discuss the implications of the new function, with emphasis on its ability to explain non-Fickian behavior, which arises because of energy dissipation events during particle deposition even in mildly heterogeneous media.

*Introduction.*—Passive transport of particles through disordered porous media is fundamental to many fields of science and engineering, including environmental tracers monitoring [1], contaminants transport in the subsurface [2], particles mixing in fluidized beds [3], and pharmaceuticals delivery [4]. The particle transport characteristics are often regarded as a signature of the swept porous structure, but their interpretation remains elusive: particle size, injection flow rate, and medium spatial heterogeneity are determining factors.

The relative importance of advection versus diffusion in establishing the particle flow distribution is summarized by the particle Péclet number,  $Pe^* = \langle v_w \rangle d_p / D_w$  (where  $\langle v_w \rangle$  is the mean velocity of the ambient fluid,  $D_w$  is its molecular diffusion coefficient, and  $d_p$  is particle diameter) [5]. The particle size spans several orders of magnitude, from molecules ( $10^{-9}$  m) to nanoparticles ( $10^{-8}$ - $10^{-6}$  m) and microparticles ( $10^{-6}$ - $10^{-3}$  m) [6]. Their propagation in the media is understood from the analysis of the probability distribution (PD) data of the longitudinal velocity [5, 7]. PDs of the longitudinal particle velocity determined experimentally commonly feature heavily tailed non-Gaussian distributions, which is regarded as the manifestation of non-Fickian transport through a heterogeneous pore system [8–11]. Indeed, similar non-Gaussian distributions have been generally observed in other granular particle systems, such as for clustered gases [12–15]. Although such experimental data are typically fitted with exponential [11, 16, 17], stretched exponential [18, 19], power-law [20, 21], or power-exponential [22] probability density functions (PDFs), our analysis suggests that such approximations might fail to capture the *entire* velocity range. In the literature, laboratory particle-tracking data for solutes, nanoparticles, and microparticles through random packs of spheres yield similar non-exponential probability decay with increasing velocity [10, 11, 23], suggesting the possibility that a universal distribution in particle kinetics might exist. The correspondent closed-form function has not yet been identified.

In this Letter, we assess the universality of passive particles kinetics in porous media. We simulate Lagrangian particle transport in a three-dimensional random packing of monodispersed spheres for  $5 \times 10^{-4} \leq Pe^* \leq 619$  and use the longitudinal velocity PD to develop a statistical model. The model qualitatively unifies particle kinetic PDs observed experimen-

tally in a closed-form formula and quantitatively explains the strength of non-Fickian behavior by key statistical parameters. We verify our Lagrangian and statistical models through comparison against particle-tracking experiments reported in the literature.

*Methodology.*—We compare experimental results of particle flow in monodispersed sphere packings obtained from nuclear magnetic resonance [10], confocal microscopy [11], and three-dimensional particle tracking velocimetry [23]. Although the experiments were conducted for different injection flow rates and particle sizes, the PD of the normalized longitudinal velocity  $v$  (particle longitudinal velocity  $v_{pL}$  rescaled by  $\langle v_w \rangle$ ) on the positive tail shows a similar trend including an initial fast decay ( $v < 1$ ), followed by a slow decay ( $1 \leq v < 3$ ), and a transition to a fast decay ( $v \geq 3$ ). One exponential or power-law function fails to describe the entire velocity range. Instead, a linear summation function  $\ln[g(v)] = a + b \times \ln(v) + c \times v^2$  (coefficients  $a > 0$ ,  $b < 0$ ,  $c < 0$ ) is attractive, because the logarithmic and quadratic terms dominate the low and high velocity regions, respectively, and their summation captures the non-exponential decay trend. We find that the correspondent  $g(v)$  is an *atypical* Nakagami- $m$  PDF of  $f_V(v)$  in Eq. (1).

The Nakagami- $m$  distribution was introduced to describe the fading signal intensity in wireless communications [24], in which case the typical shape parameter  $m$  is  $\geq 0.5$  and the PDF is characterized by a *rise* to a maximum followed by a slow decay transitioning to a fast decay. To capture the fast *decay* of low particle velocity as observed experimentally [23] and numerically [16, 19], necessarily  $0 < m < 0.5$ , according to the constraint  $b < 0$  in  $g(v)$ . Therefore, in the remainder of the Letter, Eq. (1) is referred to as an *atypical* Nakagami- $m$  PDF for particle velocity  $v$ . In Eq. (1),  $\Omega$  is the scale parameter and  $\Gamma(\cdot)$  is the Gamma function.

$$f_V(v; m, \Omega) = \frac{2m^m}{\Gamma(m)\Omega^m} v^{2m-1} \exp\left(-\frac{m}{\Omega} v^2\right), \quad (1)$$

$$\forall v > 0, 0 < m < 0.5, \Omega > 0$$

To test whether Eq. (1) is the universal law for particle longitudinal velocity, we perform numerical simulations

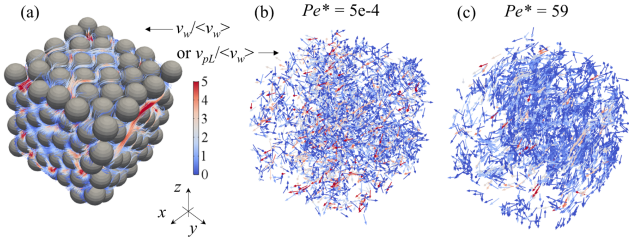


FIG. 1. (a) Fluid velocity field in 3D random jammed packing of monodispersed spheres. Particle spatial distributions at (b)  $Pe^* = 5 \times 10^{-4}$  (Solute at  $Pe = 128$ ) and (c)  $Pe^* = 59$  (MP at  $Pe = 1027$ ) in the pore structure at  $t = 10\tau$ . Ends of arrow tails denote the particles' instantaneous position. The arrows denote the direction of particle velocity vectors  $\mathbf{v}_p = v_{pL}\mathbf{L} + v_{py}\mathbf{y} + v_{pz}\mathbf{z}$ . Their color denotes the scaled particle longitudinal velocity ( $v = v_{pL}/\langle v_w \rangle$ ). Stronger deposition ( $v \approx 0$ ) is observed in (c) than (b).

of particles transport through a random jammed packing of spheres. We generate the sphere pack (porous media) by a modified Lubachevsky-Stiller algorithm [25], in which points randomly distributed within a cubic simulation box of edge length  $L \approx 6d_g$  grow into non-overlapping monodispersed spheres of diameter  $d_g = 3.6$  mm. The procedure yields 220 spheres, an average pore size  $l = 1.18$  mm, and a porosity of 36%, as shown in Fig. 1(a). The spheres are modeled as Nafion NR50 pellets, with zeta potential  $-2.23$  mV [8, 26]. We simulate incompressible steady viscous fluid flow (isopropanol with deionized water of 42 vol/vol %; fluid density  $\rho_w = 786$  kg/m<sup>3</sup>, kinematic viscosity  $\kappa_w = 1.84 \times 10^{-6}$  m<sup>2</sup>/s) at temperature  $T = 293.15$  K through the sphere pack by solving the Navier-Stokes equations with no-slip fluid-sphere boundary conditions (using the software COMSOL Multiphysics®). Periodic boundaries are specified on the six opposing faces of the simulation box. A constant pressure gradient is imposed along the longitudinal direction. Different pressure gradients yield different injection flow rates and different pore Péclet numbers  $Pe = \langle v_w \rangle l / D_w$  [7]. For all cases studied, the maximum Reynolds number ( $Re = \langle v_w \rangle l / \kappa_w$ ) is 10, and therefore our calculations are conducted below the limit of the laminar regime in porous media ( $Re \approx 180$ ) [27].

Following the methodology described by [28], we simulate Lagrangian particles transport within the flow field. The particles considered include fluorescein (solute), nanoparticles (NPs), and microparticles (MPs), of diameter  $d_p = 5$  nm, 159 nm, and 68  $\mu$ m, respectively, and mass density  $\rho_p = 786$ ,  $10^3$ , and  $10^3$  kg/m<sup>3</sup> [8, 29]. The range of particle size and pressure gradient enables probing a wide range of  $Pe^*$ . NPs and MPs are treated as negatively-charged polyethylene particles with a zeta potential of  $-45$  mV [8]. In each simulation, 3000 particles of the same type are studied. Particle size exclusion is neglected as the ratio between particle size to pore size is small. Particles are initially distributed at the upstream pressure and their initial velocity is assumed as the local fluid velocity. After a particle ensemble is released, the particles velocities change due to the exerted net force ( $\mathbf{F}_{net}$ ) at each timestep.

The maximum timestep is set to 0.001 s. Solute particles are subject to hydrodynamic drag and diffusive forces; NPs and MPs experience hydrodynamic drag, diffusive, and gravity (buoyancy) forces, particle-particle interactions (Coulomb and Van der Waals (VdW) forces), and particle-sphere interactions (London-VdW and electrical double layer forces). The drag force is corrected for the wall effect [30]. Diffusive boundary conditions are imposed after particle collisions to spheres. The instantaneous particle velocity vector ( $\mathbf{v}_p$ ) is obtained by solving Newton's second law:  $d\mathbf{v}_p/dt = \mathbf{F}_{net}/m_p$ , where  $m_p$  is particle mass. The observation time is scaled by the characteristic advection time  $\tau = l/\langle v_w \rangle$  [16]. The reliability of the above algorithm was established by reproducing the experimental data for one-dimensional particle propagators from particle tracking velocimetry [31] (see Fig. S1 in Supplemental Material).

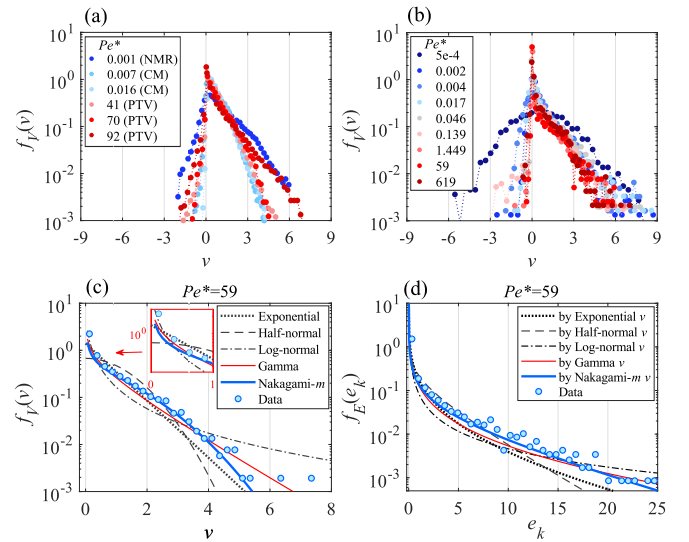


FIG. 2. (a) Experimental probability distributions of  $v$  measured at different  $Pe^*$  via nuclear magnetic resonance (NMR) [10], confocal microscopy (CM) [11], and particle tracking velocimetry (PTV) [23]. (b) Probability distributions of  $v$  obtained in this study by Lagrangian simulations at different  $Pe^*$ . (c) Simulation data of  $v$  at  $Pe^* = 59$  (MP at  $Pe = 1027$ ) (symbols) estimated by the atypical Nakagami- $m$  PDF (blue) and other PDFs (see legend). (d) Particle kinetic energy ( $e_k$ ) PDF predictions by the atypical Nakagami- $m$   $v$  (blue) versus other  $v$  PDFs (see legend) compared to simulated  $e_k$  data (symbols) at  $Pe^* = 59$ .

*Results: Statistical comparisons.*—We obtain the PD for simulated  $v$  by sampling the ensemble of particles. Three-dimensional representations of such distributions are illustrated in Figs. 1(b) and 1(c) at two different  $Pe^*$ . The long-time ( $t = 10\tau$ ) PDs for  $5 \times 10^{-4} \leq Pe^* \leq 619$  are shown in Fig. 2(b). As  $Pe^*$  increases, the PDs transition from Gaussian to non-Gaussian distributions featuring a sharp peak at near-zero velocities and heavy right tails. The results agree with the experiments shown in Fig. 2(a). Based on the maximum-likelihood (ML) estimation, the tail over positive  $v$  is fitted with the atypical Nakagami- $m$  PDF and other widely used decay PDFs such as exponential, half-normal,

log-normal, and gamma distributions [32]. In the ML fitting with the atypical Nakagami- $m$  distribution,  $m$  and  $\Omega$  are obtained by solving the derivatives of the logarithmic likelihood function ( $\mathcal{L}$ ):  $\mathcal{L}(v_i; m, \Omega, N) = N \ln \left[ \frac{2}{\Gamma(m)} \left( \frac{m}{\Omega} \right)^m \right] + (2m - 1) \sum_{i=1}^N \ln v_i - \frac{m}{\Omega} \sum_{i=1}^N v_i^2$  [33], where  $v_i$  is the velocity observation of the  $i$ th particle in the population of  $N$  particles. For all cases studied when  $Pe^* \in [5 \times 10^{-4}, 619]$ , out of all the functions considered, the atypical Nakagami- $m$  distribution is the one most consistent with the entire range of velocity data up to the noise floor. An example shown in Fig. 2(c) at  $Pe^* = 59$  along with the cases shown in Fig. 3(a) and Fig. S3 (see Supplemental Material) at other  $Pe^*$  values confirms the general applicability for this function.

To further test whether Eq. (1) is the most appropriate function (out of those PDFs considered here), we generate its random velocities to predict particles relative kinetic energy ( $e_k$ ), defined as the longitudinal kinetic energy ratio of a particle ( $E_{kPL}$ ) to the mean fluid ( $E_{kw}$ ) of the same particle volume  $V_p$ :  $e_k = E_{kPL}/E_{kw}$  where  $E_{kPL} = \frac{1}{2} \rho_p v_{pL}^2 V_p$  ( $\forall v_{pL} > 0$ ) and  $E_{kw} = \frac{1}{2} \rho_w \langle v_w \rangle^2 V_p$ . We derive  $e_k = \chi v^2$ , where  $\chi = \rho_p / \rho_w$  is the particle specific gravity. By imposing  $f_E(e_k) de_k = f_V(v) dv$  ( $\forall v > 0$ ) in Eq. (1), the PDF for  $e_k$  yields

$$f_E(e_k; m, \Omega) = \frac{1}{\Gamma(m)} \left( \frac{m}{\chi \Omega} \right)^m e_k^{m-1} \exp \left( -\frac{m}{\chi \Omega} e_k \right), \quad (2)$$

$$0 < m < 0.5, \Omega > 0.$$

We use the  $m$  and  $\Omega$  values estimated from the ML atypical Nakagami- $m$  fit of  $v$  as inputs for Eq. (2). Predictions from Eq. (2) are then compared against their counterparts obtained by simulation for all  $Pe^*$ . The example shown in Fig. 2(d) ( $Pe^* = 59$ ) demonstrates the predictive ability of the PDF. For comparison, we follow the same procedure assuming  $v$  is described by exponential, half-normal, log-normal, and gamma distributions and derive their respective PDFs for  $e_k$ , as presented in Supplemental Material. The resultant predictions for  $e_k$  are plotted in Fig. 2(d) at  $Pe^* = 59$  and in Fig. S4 (see Supplemental Material) at other  $Pe^*$ . The predictions obtained assuming atypical Nakagami- $m$   $v$  are the most reliable, supporting our hypothesis that atypical Nakagami- $m$  distributions statistically capture particle velocity distributions for passive particle transport through the porous media considered here.

*Discussions: Physical significance.*—In an attempt to identify the physical meaning of the atypical Nakagami- $m$  velocity distributions for particles flow through porous media, we resort to the statistical definitions of the scale parameter  $\Omega$  and of the shape parameter  $m$ . These parameters are defined as expectation  $E[\cdot]$  and standard deviation  $\sigma[\cdot]$  of squared velocity variables:  $\Omega = E[v^2]$  and  $m = (E[v^2]/\sigma[v^2])^2$  [24].

Because  $\Omega$  relates to  $v^2$ , we associate it with the mean kinetic energy ( $E[e_k]$ ) as  $\Omega = E[e_k]/\chi$ . By analyzing the evolution of simulated  $E[e_k]$  with observation times ( $t$ ), we observe: When the particles are initially released from the upstream pressure, they acquire energy from the ambient fluid; the  $E[e_k]$  value increases during the first characteristic advection time ( $0 < t < \tau$ ). As some of the particles transport near

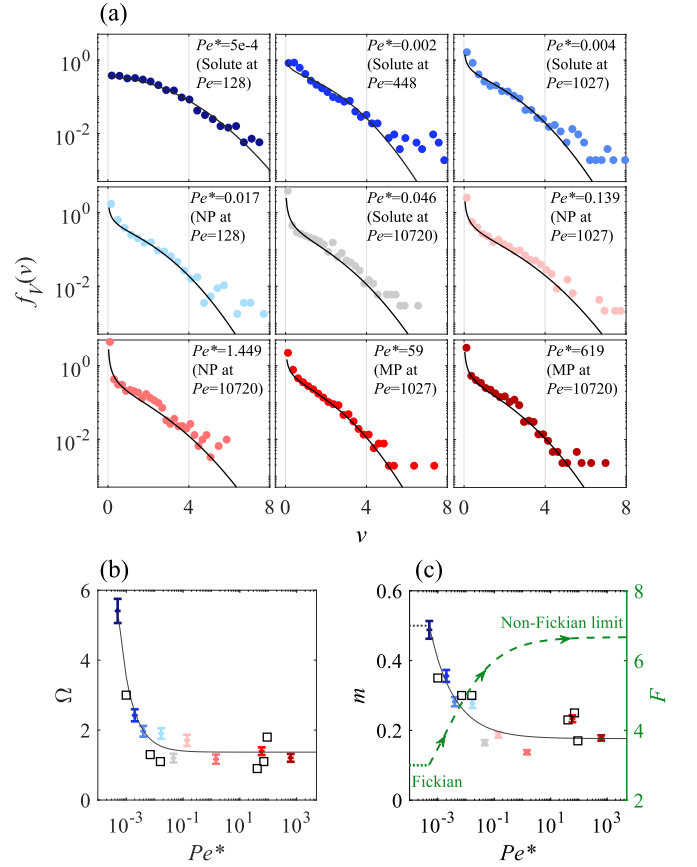


FIG. 3. (a) Atypical Nakagami- $m$  fit (solid line) of  $v$  data (symbols) from Lagrangian simulations at increasing  $Pe^* \in [5 \times 10^{-4}, 619]$ . (b) Estimates of scale parameter ( $\Omega = E[e_k]/\chi$ ) and (c) shape parameter  $m = (F - 1)^{-1}$  from simulations (symbols with 95% confidence interval error bars) and experiments (squares) from Fig. 2(a). The power-law scaling  $\Omega$  is obtained by fitting simulation data as a function of  $Pe^*$ :  $\Omega = 0.004239 \times (Pe^*)^{-0.9019} + 1.37$  and  $m = 0.007877 \times (Pe^*)^{-0.4867} + 0.1763$ .  $F$  is plotted as  $F = 1 + m^{-1}$  (dashed line) where  $m$  values are estimated from the power-law scaling.

stagnation zones and deposit due to gravity or interactions with the porous media,  $E[e_k]$  decreases as the observation time increases ( $t \geq \tau$ ). Therefore, the likelihood of particle deposition determines the mean energy dissipation and  $\Omega$  at long times (e.g.,  $t = 10\tau$ ). Our analysis reveals a power-law scaling  $\Omega \sim (Pe^*)^{-0.9019}$ , as shown in Fig. 3(b). Also presented are the estimated  $\Omega$  values from the experimental data shown in Fig. 2(a), which are in good agreement with the anticipated power-law relation. When  $Pe^* \leq 1$ ,  $\Omega$  decreases as  $Pe^*$  increases, reflecting that particles are more likely to deposit as  $Pe^*$  increases. When  $Pe^* > 1$ , the likelihood of particle deposition and correspondingly  $\Omega$  only show weak dependence on  $Pe^*$ . Visual inspection of Fig. 1(b) ( $Pe^* = 5 \times 10^{-4}$ ) and Fig. 1(c) ( $Pe^* = 59$ ) confirms this general trend, as we observe more pronounced particles deposition ( $v \approx 0$ ) in the latter case and, accordingly, a lower value of  $\Omega$ . More comparisons are presented in Supplemental Material (Fig. S2).

Because  $m$  relates to the fourth power of  $v$ , we associate it with the flatness of the PDF ( $F = E[v^4]/(E[v^2])^2$  [34]), which can in turn be used as an indicator of the strength of non-Fickian behavior [34, 35]. For example, when  $\forall v > 0$ ,  $F = 3$  indicates a half-normal tailing (Gaussian distribution) in which diffusive forces dominate the transport of particles, as expected for a Fickian behavior. By the definition of  $m$  and  $F$ , we obtain  $m = (F - 1)^{-1}$ , which shows that  $m$  is a direct indicator of non-Fickianity, with  $m = 0.5$  representing Fickian behavior.

Our results suggest that at  $Pe^* = 5 \times 10^{-4}$ , the particle velocity distribution is closest to the half-normal distribution ( $m = 0.488$ ) with particles exhibiting near-Fickian behavior. As shown in Fig. 3(c), the relation between  $m$  and  $Pe^*$  is found to obey a power-law scaling  $m \sim (Pe^*)^{-0.4867}$ . When  $Pe^* \leq 1$ , as  $Pe^*$  increases,  $m$  and  $F$  deviate from  $m = 0.5$  and  $F = 3$ , respectively, and a PDF peak emerges near zero velocity (Fig. 3(a)); the decay from this peak becomes sharper when  $Pe^*$  increases, exhibiting a more pronounced non-Fickian signature. When  $Pe^* \geq 10$ , the strength of the non-Fickian behavior reaches an upper limit. Also presented in Fig. 3(c) are the estimated  $m$  values from the experimental data shown in Fig. 2(a), which agree well with the expected power-law relation. The transition from near-Fickian to non-Fickian behavior is rapid in a narrow range of  $Pe^*$  from  $5 \times 10^{-4}$  to 0.002, suggesting that non-Fickian behavior in particle flow is rather the rule and not the exception.

The ability to relate the statistical parameters  $\Omega$  and  $m$  to physical behavior allows us to identify the culprit of non-Fickian behavior as particle deposition. Particles that tend to deposit lose kinetic energy (lower  $\Omega$ ) at long times, yielding higher probabilities of low velocity and a sharper decay (lower  $m$ ); consequently, these particles exhibit strong non-Fickian behavior (higher  $F$ ). Prediction for non-Fickian behavior of particles could therefore rely on our knowledge of the cause for particle deposition, such as the synergy between injection flow rate and particle type (size, density, and surface functionality). For example, NPs and MPs are more likely than solutes to exhibit non-Fickian behavior due to a higher likelihood of deposition by gravity and particle-sphere attractions. Additional insights could be obtained by comparing the results obtained for  $Pe^* = 0.017$  (NP at  $Pe = 128$ ) versus  $Pe^* = 0.046$  (Solute at  $Pe = 10720$ ). Despite the fact that the solute is less likely to deposit by weak gravitation and surface functionality, the strong hydrodynamic condition leads to frequent collisions of solute particles against the sphere pack, increasing the likelihood of deposition and resulting in more pronounced non-Fickian behavior compared to the NPs. Based on our model, high particle density, surface functionality complementary to that of the porous medium, and high injection rate could lead to pronounced non-Fickian behavior because they favor deposition.

Non-Fickian behavior has been traditionally attributed to fluid stagnation and is known to be pronounced in heterogeneous porous media [7, 9, 36–38]. We find here that for transport with suspended particles, the impact of fluid stagnation is

manifested in particle deposition. We show that fluid stagnation is *not* the only reason for non-Fickian behavior because other factors that can facilitate deposition may be independent of the pore structure. For example, we observe here strikingly non-Fickian behavior through monodispersed packing of spheres, for which heterogeneity is relatively mild.

In the Fickian limit, the statistical model represented by Eqs. (1) and (2) readily yields the Maxwell-Boltzmann (MB) distribution. When the particles are perfectly entrained in the flow stream ( $\chi = 1$ ) and the half-normal tailing is achieved ( $F = 3$ ), implementing four steps [(1) using dimensional velocity,  $v_{pL} = v \times \langle v_w \rangle$ ; (2) deriving PDFs for dimensional velocity  $f_V(v_{pL}) = f_V(v)dv/dv_{pL}$  and kinetic energy  $f_E(E_{kpL}) = f_E(e_k)de_k/dE_{kpL}$ ; (3) substituting  $E(E_{kpL}) = \frac{1}{2}m_p E(v_{pL}^2) = \frac{1}{2}k_B T$  (where  $k_B$  is the Boltzmann constant;  $T$  is temperature), based on the theorem of equipartition of energy with one-degree of freedom; and (4) rearranging the scale parameter  $\Omega = E(v_{pL}^2)/\langle v_w \rangle^2 = k_B T/m_p \langle v_w \rangle^2$ ] yields:

$$f_V(v_{pL}) = \sqrt{\frac{2m_p}{\pi k_B T}} \exp\left(-\frac{m_p v_{pL}^2}{2k_B T}\right), \forall v_{pL} > 0, \quad (3)$$

and

$$f_E(E_{kpL}) = \sqrt{\frac{1}{\pi E_{kpL} k_B T}} \exp\left(-\frac{E_{kpL}}{k_B T}\right). \quad (4)$$

Equations (3) and (4) represent the MB distributions in velocity ( $v_{pL}$ ) and kinetic energy ( $E_{kpL}$ ) with one-degree of freedom for all the velocities being positive (i.e.,  $\int_0^{+\infty} f_V(v_{pL})dv_{pL} = 1$ ). By comparing Eqs. (1) and (2) to the MB velocity distributions, we find that the key to capturing non-Fickian kinetics is the non-linear term  $v^{2m-1}$  in Eq. (1), which, in turn, corresponds to the term  $\ln(v)$  of the linear summation  $\ln[g(v)]$  presented at the beginning of the Letter, suggesting that the atypical Nakagami- $m$  distribution has its unique mathematical advantage.

*Conclusions.*—The model presented here captures a universal distribution for non-Fickian particle kinetics. We show that the shape of velocity PDFs directly indicates non-Fickian signatures of particle transport in porous media and further demonstrate how the strength of non-Fickian behavior is impacted by the likelihood of particle deposition. When particles transport conditions favor their deposition, non-Fickian behavior is anticipated in porous media, whether mildly or strongly heterogenous. The relations between the statistical parameters ( $m, \Omega$ ) and  $Pe^*$  could be efficient predictors for transport signatures in various media. The proposed distribution function converges to the Maxwell-Boltzmann distribution when the conditions yield Fickian behavior. Our statistical model might also be useful for developing kinetic theories in other particulate systems that exhibit striking non-Gaussian distributions, such as clustered granular gases [12–15].

This work is supported by the Science4CleanEnergy European research consortium funded by European Union's Horizon 2020 research and innovation programme, under Grant

Agreement No.764810(S4CE). Generous allocations of computing time were provided by the University College London Research Computing Platforms Support (Kathleen). We are indebted to M. Holzner and M. Carrel of ETH Zürich for offering 3D particle tracking velocimetry experimental data as well as V.L. Morales of the University of California, Davis for helpful correspondence.

---

\* d.fan@ucl.ac.uk

† a.striolo@ucl.ac.uk

- [1] R. Liao, P. Yang, W. Wu, D. Luo, and D. Yang, *Environmental science & technology* **52**, 1695 (2018).
- [2] T. Bhattacharjee and S. S. Datta, *Nature communications* **10**, 1 (2019).
- [3] H. Bi, N. Ellis, I. Abba, and J. Grace, *Chemical Engineering Science* **55**, 4789 (2000).
- [4] V. P. Torchilin, *Nature reviews Drug discovery* **13**, 813 (2014).
- [5] D. Kandhai, D. Hlushkou, A. G. Hoekstra, P. M. Sloot, H. Van As, and U. Tallarek, *Physical review letters* **88**, 234501 (2002).
- [6] J. Kreuter, *Journal of anatomy* **189**, 503 (1996).
- [7] B. Bijeljic, P. Mostaghimi, and M. J. Blunt, *Physical review letters* **107**, 204502 (2011).
- [8] V. L. Morales, M. Dentz, M. Willmann, and M. Holzner, *Geophysical Research Letters* **44**, 9361 (2017).
- [9] B. Bijeljic, A. Raeini, P. Mostaghimi, and M. J. Blunt, *Physical Review E* **87**, 013011 (2013).
- [10] Y. Kutsovsky, L. Scriven, H. Davis, and B. E. Hammer, *Physics of Fluids* **8**, 863 (1996).
- [11] S. S. Datta, H. Chiang, T. Ramakrishnan, and D. A. Weitz, *Physical review letters* **111**, 064501 (2013).
- [12] J. Van Zon and F. MacKintosh, *Physical review letters* **93**, 038001 (2004).
- [13] K. Harth, T. Trittel, S. Wegner, and R. Stannarius, *Physical review letters* **120**, 214301 (2018).
- [14] A. Prevost, D. A. Egolf, and J. S. Urbach, *Physical review letters* **89**, 084301 (2002).
- [15] J. Olafsen and J. Urbach, *Physical review letters* **81**, 4369 (1998).
- [16] P. de Anna, T. Le Borgne, M. Dentz, A. M. Tartakovsky, D. Bolster, and P. Davy, *Physical review letters* **110**, 184502 (2013).
- [17] K. Alim, S. Parsa, D. A. Weitz, and M. P. Brenner, *Physical review letters* **119**, 144501 (2017).
- [18] F. Rouyer, J. Martin, and D. Salin, *Physical review letters* **83**, 1058 (1999).
- [19] M. Siena, M. Riva, J. Hyman, C. L. Winter, and A. Guadagnini, *Physical Review E* **89**, 013018 (2014).
- [20] P. de Anna, B. Quaipe, G. Biroso, and R. Juanes, *Physical Review Fluids* **2**, 124103 (2017).
- [21] G. R. Gudon, F. Inzoli, M. Riva, and A. Guadagnini, *Physical Review E* **100**, 043101 (2019).
- [22] M. Matyka, J. Goembiewski, and Z. Koza, *Physical Review E* **93**, 013110 (2016).
- [23] M. Carrel, V. L. Morales, M. Dentz, N. Derlon, E. Morgenroth, and M. Holzner, *Water resources research* **54**, 2183 (2018).
- [24] M. Nakagami, The m-distribution a general formula of intensity distribution of rapid fading, in *Statistical methods in radio wave propagation* (Elsevier, 1960) pp. 3–36.
- [25] M. Skoge, A. Donev, F. H. Stillinger, and S. Torquato, *Physical Review E* **74**, 041127 (2006).
- [26] H. Zhang, J. Pan, X. He, and M. Pan, *Journal of applied polymer science* **107**, 3306 (2008).
- [27] D. Seguin, A. Montillet, and J. Comiti, *Chemical engineering science* **53**, 3751 (1998).
- [28] H. Ma, J. Pedel, P. Fife, and W. P. Johnson, *Environmental science & technology* **43**, 8573 (2009).
- [29] G. Mikutis, C. A. Deuber, L. Schmid, A. Kittilä, N. Lobsiger, M. Puddu, D. O. Asgeirsson, R. N. Grass, M. O. Saar, and W. J. Stark, *Environmental science & technology* **52**, 12142 (2018).
- [30] J. Happel and H. Brenner, *Low Reynolds number hydrodynamics: with special applications to particulate media*, Vol. 1 (Springer Science & Business Media, 2012).
- [31] M. Holzner, V. L. Morales, M. Willmann, and M. Dentz, *Physical Review E* **92**, 013015 (2015).
- [32] F. James, *Statistical methods in experimental physics* (World Scientific Publishing Company, 2006).
- [33] J. Cheng and N. C. Beaulieu, *IEEE Communications letters* **5**, 101 (2001).
- [34] J. Olafsen and J. S. Urbach, *Physical Review E* **60**, R2468 (1999).
- [35] G. Baxter and J. Olafsen, *Nature* **425**, 680 (2003).
- [36] M. Dentz and D. M. Tartakovsky, *Geophysical research letters* **33** (2006).
- [37] T. Le Borgne, M. Dentz, and J. Carrera, *Physical review letters* **101**, 090601 (2008).
- [38] M. Dentz, M. Icardi, and J. J. Hidalgo, *Journal of Fluid Mechanics* **841**, 851 (2018).